Suppression of underlying neuronal fluctuations mediates EEG slowing during general anaesthesia

Axel Hutt, Jeremie Lefebvre, Darren Hight, Jamie Sleigh

Suppression of underlying neuronal fluctuations mediates EEG slowing during general anaesthesia

Axel Hutt[1], Jérémie Lefebvre[2], Darren Hight[3 4], Jamie Sleigh[3,*]

[1] *Department FE 12 – Data Assimilation , Deutscher Wetterdienst, 63067 Offenbach am Main, Germany*
Department of Mathematics and Statistics, University of Reading, Reading RG6 6AX,UK

[2] *Krembil Research Institute, University Health Network, Toronto, Ontario M5T 2S8, Canada*
Department of Mathematics, University of Toronto, Toronto, Ontario M5T 2S8, Canada
Institute of Biomaterials and Biomedical Engineering, University of Toronto, Toronto, Ontario M5T 2S8, Canada

[3] *Department of Anaesthesiology, Waikato Clinical Campus, University of Auckland, Hamilton 3240, New Zealand*

[4] *Department of Anaesthesiology and Pain Therapy, University Hospital Bern, Inselspital, Bern, Switzerland*

Short title: Random fluctuations slow anaesthesia EEG

Keywords : anaesthesia, noise, functional fragmentation, alpha-activity

Corresponding author:
Axel Hutt
Deutscher Wetterdienst
Department FE12- Data Assimilation
Frankfurter Strasse 135
63067 Offenbach am Main , Germany
Tel.: +49 69 80622750 , Email: digitalesbad@gmail.com

Abstract

The physiological mechanisms by which anaesthetic drugs modulate oscillatory brain activity remain poorly understood. Combining human data, mathematical and computational analysis of both spiking and mean-field models, we investigated the spectral dynamics of encephalographic (EEG) beta-alpha oscillations, observed in human patients undergoing general anaesthesia. The effect of anaesthetics can be modelled as a reduction of neural fluctuation intensity, and/or an increase in inhibitory synaptic gain in the thalamo-cortical circuit. Unlike previous work, which suggested the primary importance of gamma-amino-butryic-acid(GABA) augmentation in causing a shift to low EEG frequencies, our analysis demonstrates that a non-linear transition, triggered by a simple decrease in neural fluctuation intensity, is sufficient to explain the clinically-observed appearance – and subsequent slowing – of the beta-alpha narrowband EEG peak. In our model, increased synaptic inhibition alone, did not correlate with the clinically-observed encephalographic spectral changes, but did cause the anaesthetic-induced decrease in neuronal firing rate. Taken together, our results show that such a non-linear transition results in functional fragmentation of cortical and thalamic populations; highly correlated intra-population dynamics triggered by anaesthesia decouple and isolate neural populations. Our results are able to parsimoniously unify and replicate the observed anaesthetic effects on both the EEG spectra and inter-regional connectivity, and further highlight the importance of neural activity fluctuations in the genesis of altered brain states.

Introduction

General anaesthesia is a widely used medical procedure in today's clinical practice. One of the main obstacles in the optimization of general anaesthesia is the limited understanding of the physiological mechanisms behind anaesthetic actions and their consequences on neural information processing.

One of the prominent effects of most commonly used anaesthetic drugs is the induction of characteristic changes in the spectral properties of electrophysiological activity across cortical brain areas and spanning multiple frequency bands (1, 2, 3, 4). These spectral changes have been used as the basis for many monitoring indices of electroencephalographic data (EEG) measured empirically during anaesthesia (5), and as such constitute one of the most reliable biomarkers of the brain's arousal state. One of the most salient spectral changes observed in clinical practice is the generation of prominent oscillatory activity in the β-frequency band (12 Hz -20 Hz) and its subsequent gradual decrease to the α-frequency band (8 Hz -12 Hz) with increasing anaesthetic concentration (6).

This slowing down in oscillatory neural activity has also been shown to correlate strongly with patients' behavioural state. Indeed, in parallel to the encephalographic deceleration from β- to α-activity, subjects' behavioural state changes from a sedated state to one of loss of responsiveness – which we may equate with loss of connected consciousness (LOC).

Previous theoretical and computational studies have developed neural network models (7, 8) as well as neural mass models (9, 10) to reproduce both β- and α-activity as observed across the different states of anaesthesia. While insightful, these studies use network models with the limiting assumptions of single anaesthetics acting on specific synaptic receptors or isolated ion channels, and do so symmetrically across all neurons in a given circuit. From a practical perspective

however, mixtures of different classes of anaesthetic agents – as opposed to only one agent – are almost always used in clinical settings to induce general anaesthesia. These combinations of anaesthetic drugs are known to interact with each other (11), and are thus likely to impact neurons and neuronal populations in heterogeneous ways. In the absence of known physiological mechanisms and detailed information about anaesthetics interactions, it remains highly challenging to model, yet properly characterize, general anaesthesia from the single neuron perspective.

In contrast to previous studies where the characteristic slowing of EEG rhythms is caused by changes in single neuron properties (often modelled as slowing of the inhibitory post-synaptic potential decay time), we here propose an alternative mechanism: that the characteristic EEG slowing is driven by *system-level interactions*. Using human data, and based on our mathematical and computational analysis of both spiking and mean-field models, we have found that the oscillatory transitions, commonly observed across sedation stages, appear to be a characteristic signature of non-linear systems undergoing a phase transition: brain dynamics switches between different dynamical states, accompanied by an amplification of coherent activity. To provide deeper insight into the neural mechanism of anaesthetics from a circuit point of view, our work shows that anaesthetic action results in an effective decrease in broadband neural activity i.e. the neural activity exchanged between neural structures involved becomes more regular and coherent. This hypothesis is in full agreement with converging lines of evidence showing that neural activity in awake human subjects and animals is highly irregular compared to activity under anaesthesia; which has very limited spatio-temporal information content (3, 12-15). A previous study (16) demonstrated nicely that spatial frontal coherence in the α-frequency increases markedly at the point when subjects lose consciousness.

We considered a thalamo-cortical circuit of spiking neurons subjected to additive external random fluctuations. When the fluctuation variance increases (as occurs during emergence from

anaesthesia), mathematical and computational analysis reveals an oscillatory transition that is a characteristic signature of non-linear systems. With decreasing variance of fluctuations (as occurs with increasing depth of anaesthesia), the opposite occurs and the system exhibits an amplification of coherent dynamics. The corresponding connectivity analysis reveals *enhanced intra*-area synchrony but a simultaneous *breakdown of inter*-area synchrony. Taken together, our results support previously proposed hypotheses (17) in which anaesthesia represents a *systemic isolation* of neural populations via a switch from globally-driven to locally-driven activity. Taken together, our results show that circuit-scale interactions – as opposed to single neuron properties - are mandatory to replicate the slowing down of EEG activity observed in human clinical data.

Materials and Methods

Experimental data

Experimental EEG data have been obtained from two patients recorded for a previous observational study (6). This had institutional ethics approval (from the New Zealand Health and Disability Ethics Committee, Ref. 12/CEN/56, 2013) and written informed consent. These patients were both female (aged 29 and 77), and had anaesthesia initiated by a single dose of propofol, and subsequently maintained by the volatile anaesthetic sevoflurane during their surgery.

The data under study was recorded from a frontal position ($Fp_{1/2}$ – Fp_z in the 10-20 system) using a Bispectral Index depth of anaesthesia monitor (BIS ®, Covidien, Boulder, CO, USA) at a sampling frequency of 128 Hz, which was then down-sampled to 100 Hz. High and low pass non-phase shifting Butterworth filters were applied to the data (at 0.25 and 48.5 Hz cutoffs respectively, both set at 3dB). We have analyzed the temporal evolution of the frequency content of experimental data

by computing its spectrogram with window width T=10s yielding a frequency resolution of 0.1Hz and window overlap of 0.1s.

Anaesthetic action of the ascending arousal system

Anaesthetics affect neural communication by modifying synaptic receptor and ion channel properties. It has been shown previously (18) that increasing anaesthetic concentrations diminish thalamic input to the cortex and reduces thalamic and cortical firing activity caused by reduced activation in the ascending arousal system (AAS, 19). Since the input to the cortex and the thalamus is rather complex and not known in all detail, we consider external input as random fluctuations with a certain mean and variance. Our underlying model considers neural population activity and the random fluctuations represent an uncorrelated synaptic bombardment with high input population firing.

To estimate the anaesthetic action on the amplitude of those random fluctuations, we consider a simple neural network describing anaesthetic action in the AAS (19, 20). Several clinically relevant anaesthetics affect GABAergic synaptic and extra-synaptic receptors in the AAS inducing phasic and tonic inhibition, respectively (2,21). For instance, GABAergic synaptic receptors are present in the AAS-structures brainstem, hypothalamus and the basal forebrain (2,21) and anaesthetics prolong their phasic response. Extra-synaptic receptors occur primarily in sub-cortical structures such the brainstem, hypothalamus and thalamus (10,22) and anaesthetics enhance the tonic inhibitory current.

The AAS exhibits a rather complex network of interacting structures that inhibit each other according to diverse direct and indirect actions. Previous experimental and theoretical studies of phasic and tonic inhibition (23) have shown that increasing the synaptic time constant and

decreasing the pre-synaptic firing rate decreases the synapses phasic response variance. This indicates decreased response mean and variance with increased anaesthetic action by prolonged post-synaptic phasic response and enhanced pre-synaptic firing reduction by tonic inhibition. To show this anaesthetic impact, we consider anaesthetic actions on both phasic and tonic inhibition in our simplified model of the AAS. To illustrate the phasic and tonic inhibition separately and clarify their action, we distribute phasic and tonic receptors over different populations. A chain of three neural populations of spiking neurons (Fig.1(a)) reflect the functional structure of AAS. The first two populations exhibit tonic and phasic inhibition and the last population sums up the output providing the random fluctuations (Fig.1(a)). These fluctuations may represent the input to thalamic structures or to the cortex.

The first population (neurons t in Fig.1(a)) includes uncoupled Leaky Integrate-and-Fire neurons (LIF) of number *N=80* with tonic inhibition (23,24). The neurons are driven by a constant input current. Such neurons may be located in brainstem structures, such as the *locus coeruleus* or *parabrachial nucleus* that project to a large part of the cortex and thalamus. Their membrane potential V_n obeys

$$C\frac{dV_n}{dt} = g_l(E_l - V_n) + g_t\,(E_t - V_n) + I\,, \qquad n = 1,..,N$$

for $V_n < \theta_n$. The thresholds θ_n are random and uniformly distributed about the mean threshold $\theta = -58mV$ in the range [-59.5mV;-56.5mV]. The reset potential is $V_{reset} = -68mV$ and an $8ms$ refractory time is chosen . The other parameters are the capacity $C = 33nF$, the constant leak conductance $g_l = 22nS$, the leak reversal potential $E_l = -76mV$ and the synaptic reversal potential $E_t = -76mV$. The external current is $I = 8nA$. The tonic conductance takes values $g_t = 0nS$, $g_t = 200nS$ and $g_t = 400nS$ that represent low, medium and high tonic anaesthetic action, respectively. In the numerical simulations, initial conditions are random and distributed uniformly

in the interval $[V_{reset} - 15mV; V_{reset} + 15mV]$. Figure 1(b) shows raster plots for the three anaesthetic levels. The larger the inhibitory tonic current, the lower is the firing rate in accordance to previous studies (23,24).

These neurons emit spikes targeting inhibitory GABAergic synapses (neurons i in Fig.1(a)) of number N with an exponential response function of time scale τ . Such synapses may be located in the hypothalamus, e.g. in the *ventrolateral preoptic nucleus,* receiving projections from the brainstem. Hence the inhibitory response potential $IPSP_m$ at post-synaptic neuron m obeys

$$\tau \frac{dIPSP_m}{dt} = -IPSP_m + s_m \, , m = 1, .. , N$$

where $s_m = 1mV$ when pre-synaptic spikes arrive and $s_m = 0$ otherwise. Anaesthetics prolong the synaptic time scale and we choose $\tau = 200ms$, $\tau = 400ms$, and $\tau = 600ms$ for low, medium and high anaesthetic impact, respectively. Figure 1(c) presents the sum of these synaptic responses $IPSP(t) = \sum_{m=1}^{N} IPSP_m \, (t)$ and reveals reduced magnitude and bias of post-synaptic currents with increased anaesthetic action.

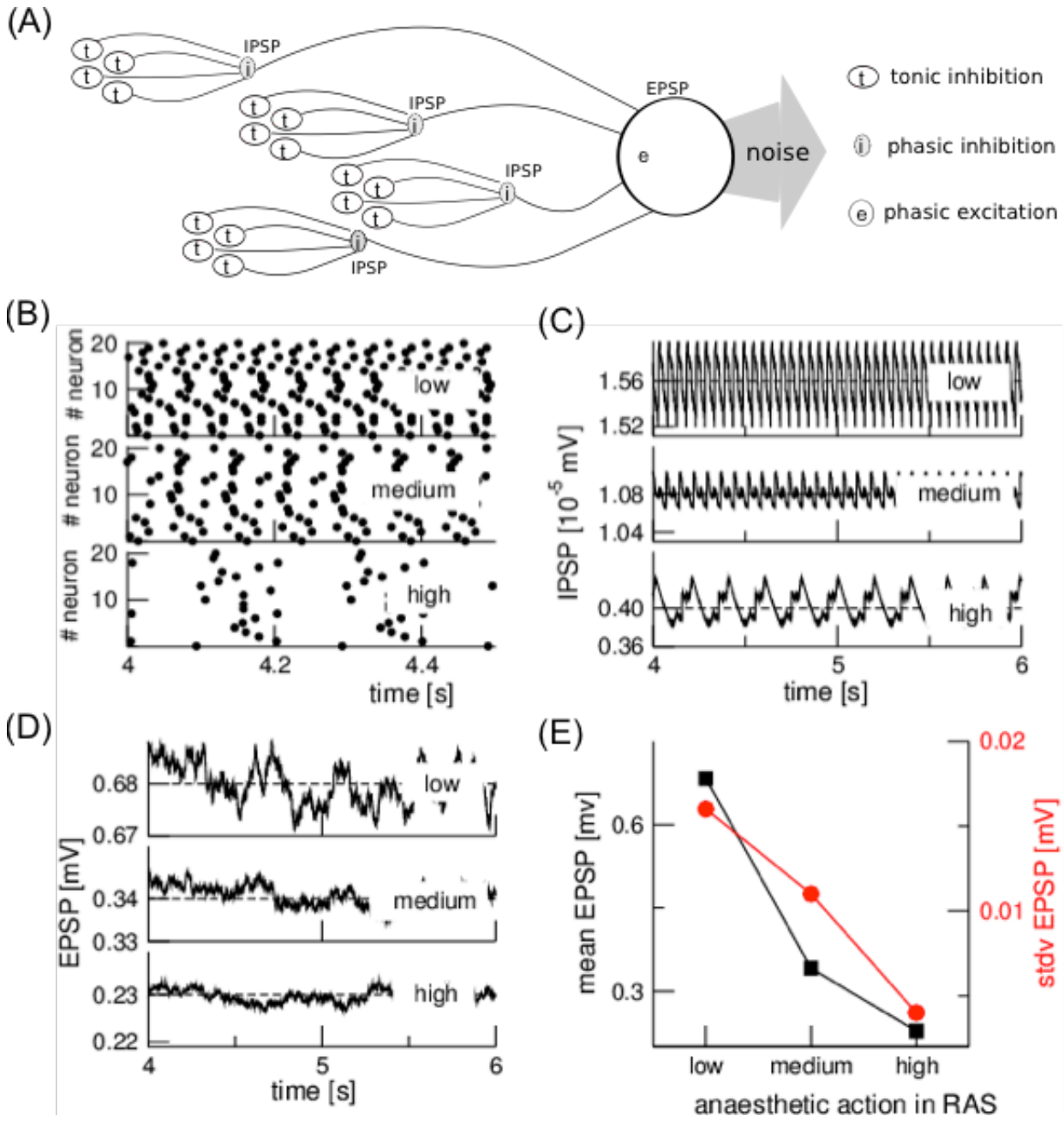

177

178 Figure 1: Effect of the ascending arousal system on cortical and thalamic activity. (A) Topology of
179 the simulated network. (B) Spike trains of the output of tonic inhibition neurons targeting phasic
180 inhibition neurons for different anaesthetic action levels (C) Inhibitory post-synaptic potentials
181 (IPSP) evoked by spike trains in (B). (D) Excitatory post-synaptic potentials (EPSP) that describes

the noise applied to the cortico-thalamic network. (E) Both mean and standard deviation of EPSP decrease with the anaesthetic action level.

The summed-up inhibitory current triggers the spike discharge in the post-synaptic neuron what is modeled as a Poisson neuron with firing rate $\lambda(t) = f[IPSP(t)]$ with the transfer function $[U] = \frac{100Hz}{1+e^{-(U-\vartheta)}}, \vartheta = 8\mu V$. We consider M=40 of such Poisson neurons whose spike discharges target excitatory synapses (neuron *e* in Fig.1(a)) with exponential response function and constant time scale of *20ms*. Such synapses may be located in the thalamus or the cortex. The sum of these excitatory responses *EPSP* represents the random fluctuations. Figure 1(d) demonstrates that stronger anaesthetic action decreases the magnitude of EPSPs and its bias. Since this EPSP describes the input of the AAS to thalamus and cortex, we summarize that increasing anaesthetic action reduces the variance of input fluctuations and its bias. These results are summarized in Fig.1(e). This finding is consistent with recent experimental evidence in rats showing that somatosensory and primary motor neurons in the anaesthetic-induced isoelectric state are fully responsive to external stimuli (55). This finding is affirmed qualitatively for humans in the same study. Since anaesthetic isoelectric states emerge under deep anaesthesia, this result demonstrates that neurons are not strongly inhibited in deep anaesthesia as it would be the case if synaptic inhibition alone would be present. We argue that anaesthetic action rather diminishes the input from AAS to these neurons and, in this way, retain their responsiveness.

In the following we modify the fluctuation variance and keep the bias constant for the frontal cortico-thalamic model. This approximation is reasonable since additional studies (not shown) revealed that the major results in the present work are invariant for small anaesthetic-induced bias adaptation. In the occipital cortico-thalamic model, we modify both the fluctuation variance and the bias. We find that the additional bias reduction is mandatory to reproduce qualitatively the occipital

power reduction. For simplicity, mentioning the fluctuation variance in the following discussion of the occipital model always implies a synchronous bias reduction.

Anaesthetic action in the frontal cortico-thalamic network

The relation proposed above between anaesthetic action and input variance does not specify in detail the relation between fluctuation variance and anaesthetic action of different anaesthetic agents in the cortex and sub-cortical structures. We hypothesize that this relationship is an effective approximation of anaesthetic action and it is valid for various combinations of anaesthetic agents. Our analysis suggests that this represents one of the major mechanisms of such pharmacological agents on thalamocortical populations.

We assume that neuron ensembles in the cortex and thalamus are subjected to endogenous, background sources of inputs $A_k^j(t) = \sqrt{2D}\,\xi_k^j(t)$ with *k=e, I, th, rtn* for the cortical excitatory (e), cortical inhibitory (i), thalamic *lateral geniculate nucleus* (th) and thalamic reticular (rtn) population (cf. Fig.2(A)). Here, $\xi_k^j(t)$ are independent random Gaussian processes with identical variance. Anaesthetic action in the cortex and thalamus is modeled by changing the level of noise or fluctuation variance D in the system with increasing anaesthetics concentration in accordance to the AAS-model. In numerical experiments, the variance either obeys the piece-wise exponential laws

$$\begin{aligned} D(t) &= D_1 e^{-t/\tau_n} + D_0\,, 0 \le t_1\,, \\ D(t) &= D_2\,, t_1 < t \le t_2\,, \\ D(t) &= D_4 e^{t/\tau_n} + D_3\,, t_2 < t \le t_3\,, \end{aligned} \qquad (1)$$

with $\tau_n, D_0, D_1, D_4 > 0, D_2 = D_1 e^{-t_1/\tau_n} + D_0, D_3 = D_2 - D_4 e^{t_2/\tau_n}$ or the linear model

$$D(t) = -mt + D_5\,, 0 \le t \le t_1 \qquad (2)$$

with $D_0 > 0, m > 0$. For Eqs. (1), we choose parameters such that $(0) = 1.01\,, D_2 = 0.01\,, D(t_3) = 0.04$ with $t_1 = t_3/2, t_2 = 0.6t_3\,, t_3 = 32.768\text{s}, \tau_n = (32786/0.16)\text{s}$. In the linear model in Eq. (2) $D_5 = 0.345$, m=0.005 with $t_1 = 32.768\text{s}$. Here, the temporal duration in both simulations is 32.768s.

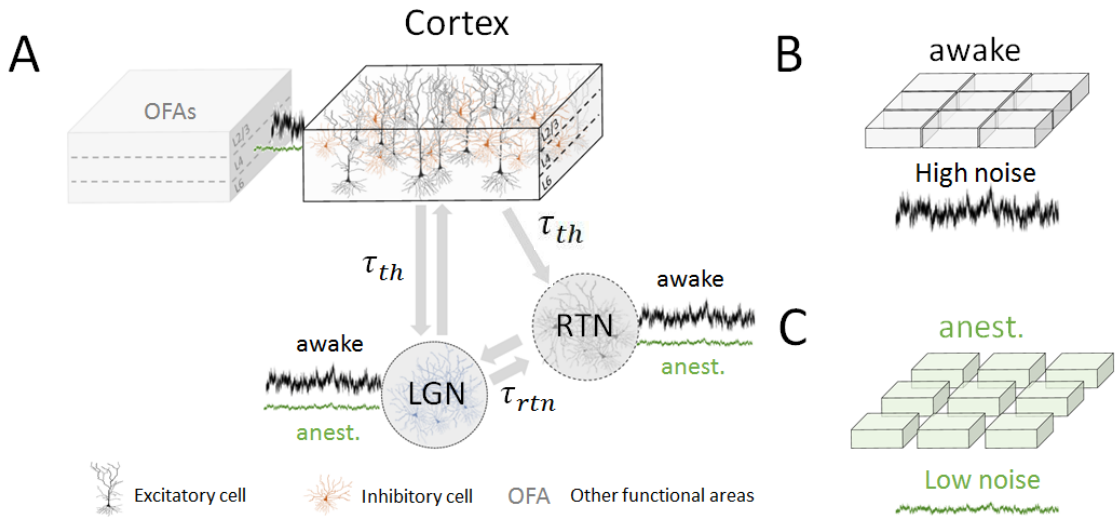

Figure 2: Illustration of thalamo-cortical network subjected to additive random fluctuations. (A) network topology (B) decreasing fluctuation variance functionally decouples the network.

We assume that this effective reduction of fluctuation variance represents the major effect of anaesthetics on the cortico-thalamic circuit. In addition to the effect of fluctuations, it has been shown in numerous experimental studies that a large variety of anaesthetic drugs inhibits neural

activity by action on GABAergic synaptic receptors. To take into account this synaptic effect , we included a prolongation of the synaptic decay time scale of inhibitory GABAergic receptors while retaining the amplitude of the synaptic inhibitory impulse response. Mathematically the synaptic decay time scale of GABAergic synapses obey

$$\tau_i(t) = \tau_i^0 p(t) .$$

When utilizing the exponential fluctuation variance model, the factor synaptic decay time scale factor obeys the linear law

$$p(t) = 1 + 2t/t_1 \ , 0 \leq t_1 ,$$

$$p(t) = 3 , t_1 < t \leq t_2 ,$$

$$p(t) = 3 - 2(t - t_2)/(t_3 - t_2) , t_2 < t \leq t_3$$

with the same times t_1 , t_2 and t_3 as in (1). The corresponding the linear model is $p(t) = 1 + 2t/t_1 \ , 0 \leq t_1$. This anaesthetic model is motivated by a previous study based on experimental data (51).

Anaesthetic action in the occipital cortico-thalamic network

The occipital anaesthetic action model is very similar to the frontal model. Since not much is known about the projection targets of the AAS to the occipital cortex, we consider a diffusive projection to the cortex via the basal forebrain (19,56) but neglect AAS stimulation of thalamic structures. To illustrate the spectral power dynamics with decreasing AAS activity, we assume the fluctuation variance D to decrease in time according to

$$D(t) = D_1 e^{-t/\tau_n} + D_0 , 0 \leq t \leq t_1$$

with $t_1 = 32.768$ s , $D(0) = 0.06$, $\tau_n = (32786/0.16)$ s and $D_0 = 0.0006$. The excitatory endogenous, fluctuating background input is $A_e^j(t) = \sqrt{2D}\,\xi_k^j(t)$, whereas other time-dependent input $A_i^j(t) = A_{th}^j(t) = A_{rtn}^j(t) = 0$. This is different to the frontal model, where all cortical and thalamic structures are driven by the AAS. Moreover, the mean excitatory input from AAS obeys the Hill equation

$$I_e(t) = -0.5 - 3/(1 + (0.7t_1/t)^4)\,, 0 \le t \le t_1\,.$$

that is a decreasing sigmoidal function with turning point at $t = 0.7t_1$. The mean input to the other structures I_i, I_{th}, I_{rtn} remain constant. To consider anaesthetic effects on synaptic inhibition, the synaptic time scale factor increases over time according to

$$p(t) = 1 + 2/(1 + (1.5t_1/\,t\,)^4)\,, 0 \le t \le t_1$$

Spiking frontal model

To understand the underlying neural mechanism of changes in EEG spectral features, we investigated a thalamo-cortical hybrid network model of Amari-type (25). The network is built of recurrently connected neural ensembles of excitatory pyramidal neurons (e) and inhibitory interneurons (i) interacting with thalamic relay (th) neurons in the Lateral Geniculate Nucleus (LGN) and thalamic reticular neurons (rtn), cf. Fig.2 (A) .

Spiking activity of those neural ensembles follow the non-homogeneous Poisson processes

$$X_e^j(t) \to Poisson\,(f[u_e^j(t)])\ ,\ X_i^j(t) \to Poisson\,(f[u_i^j(t)])$$

$$X_{th}^j(t) \to Poisson\,(f[u_{th}^j(t)])\ ,\ X_{rtn}^j(t) \to Poisson\,(f[u_{rtn}^j(t)])$$

where $X^j_{e,i,th,rtn}(t) = \sum_{\{t_l\}} \delta^j_{e,i,th,rtn}(t - t_l)$ is the spike train of the j^{th} ensemble patch in the respective population. The ensemble response function $f[u] = (1 + \exp\{-\beta(u - h)\})^{-1}$ represents a saturating firing rate function with gain β =150 and threshold h =0.1. The average potentials of ensemble j of excitatory and inhibitory neurons $u^j_e(t)$ and $u^j_i(t)$, respectively, and the thalamic potentials $u^j_{th}(t)$ and $u^j_{rtn}(t)$ obey

$$\alpha_e^{-1}\frac{du^j_e(t)}{dt} = -u^j_e(t) + b\, v^j_e(t) + S^j_{e\to e}(t) + S^j_{i\to e}(t) + S_{th\to e}(t-\tau_{th}) + I_e + A^j_e(t) \quad (3)$$

$$\alpha_i^{-1}\frac{du^j_i(t)}{dt} = -u^j_i(t) + b\, v^j_i(t) + S^j_{e\to i}(t) + S^j_{i\to i}(t) + S_{th\to i}(t-\tau_{th}) + I_i + A^j_i(t)$$

$$\alpha_{th}^{-1}\frac{du^j_{th}(t)}{dt} = -u^j_{th}(t) + b\, v^j_{th}(t) + S^j_{e\to \mathrm{th}}(t-\tau_{th}) + S^j_{rtn\to th}(t-\tau_{rtn}) + I_{th} + A^j_{th}(t)$$

$$\alpha_{rtn}^{-1}\frac{du^j_{rtn}(t)}{dt} = -u^j_{rtn}(t) + b\, v^j_{rtn}(t) + S^j_{e\to rtn}(t-\tau_{th}) + S^j_{th\to rtn}(t-\tau_{rtn}) + I_{rtn} + A^j_{rtn}(t)$$

$$a^{-1}\frac{dv^j_e(t)}{dt} = -v^j_e(t) + u^j_e(t)\ ;\ a^{-1}\frac{dv^j_i(t)}{dt} = -v^j_i(t) + u^j_i(t)$$

$$a^{-1}\frac{dv^j_{th}(t)}{dt} = -v^j_{th}(t) + u^j_{th}(t)\ ;\ a^{-1}\frac{dv^j_{rtn}(t)}{dt} = -v^j_{rtn}(t) + u^j_{rtn}(t)$$

where $v^j_n(t)$ refers to corresponding adaptation currents, b is the adaptation gain and $S^j_{n\to m}$ are synaptic inputs from population n to population m. The variables $u^j_n(t)$ represent the Local Field Potential that would be measured with an implanted electrode in population $n = e, i, th, rtn$. The terms I_n are constant bias currents and A^j_n are random external input currents. Cortico-thalamic interactions are delayed by a propagation delay τ_{th}, while we have also included an interaction delay τ_{rtn} between LGN and the reticular population. In addition, local, distance-dependent propagation delays are also included within the cortical populations. Using these, the resulting integrated synaptic inputs to the neurons are given by

$$S^{j}_{n\to m}(t) \quad = N_n^{-1} \sum_{k=1}^{N_n} W^{jk}_{n\to m} \cdot E^{k}_{nm}\left(t - \tau^{jk}\right).$$

The individual propagation delays are given by $\tau^{jk} = \Delta^{jk}/c$, where c is a finite conduction velocity and Δ^{jk} is the spatial distance between ensemble patch of number j and k. Ensembles are distributed randomly and uniformly within a one dimensional spatial domain Ω of length $|\Omega|$. Average post-synaptic potentials $E^{k}_{n}(t)$ are computed as input spike trains convolved with exponential synapses with time constant τ_m

$$E^{k}_{nm}(t) = \int_{o}^{t} X^{k}_{n}(s)\ \frac{1}{\tau_m} e^{-(t-s)/\tau_m}\ ds\ .$$

As pointed out above, $\tau_i = const$ or $\tau_i = \tau_i(t)$ in two studies. Recurrent synaptic weights amongst ($W^{jk}_{n\to n}$) and between ($W^{jk}_{n\to m}$) excitatory and inhibitory populations exhibit sparse Gaussian profiles

$$W^{jk}_{n\to m}(\rho) = \frac{w^{o}_{n\to m}(\rho)}{\sqrt{2\,\pi\ \ \sigma^{2}_{n\to m}}}\ \exp\left[-\frac{\left(\Delta^{jk}\right)^{2}}{2\ \ \sigma^{2}_{n\to m}}\right]$$

where $w^{o}_{n\to m}(\rho) = w^{o}_{n\to m} \neq 0$ with probability ρ. Model constants are given in Table 1. The numerical integration step is $\Delta t = 0.001$s and all variables have been initialized in $t \in [-\tau; 0]$ to $u_n, v_m = 0$ with the maximum delay time τ.

Table 1: Table of Model Parameters

Symbol	Definition			Symbol	Definition	
Ω	Network spatial extent [mm]	10		ρ	Connection probability	0.2
N_e	Number of excitatory cells	800		$w^{o}_{e\to e}$	Synaptic connection strength	12
N_i	Number of inhibitory cells	200		$w^{o}_{e\to i}$	Synaptic connection strength	-25
N_{th}	Number of thalamic cells	200		$w^{o}_{i\to e}$	Synaptic connection strength	25
N_{rtn}	Number of reticular cells	200		$w^{o}_{i\to i}$	Synaptic connection strength	-12
β	Neural response function gain [1/mV]	150		$w^{o}_{e\to th}$	Synaptic connection strength	5

h	Firing rate threshold [Hz]	1		$w^o_{e\to rtn}$	Synaptic connection strength	5
τ_m	mean time constant [s]	1		$w^o_{th\to e}$	Synaptic connection strength	35
α_e	mean rate constant – excitatory cortical cells [Hz]	1.0		$w^o_{th\to i}$	Synaptic connection strength	-10
α_i	mean rate constant – inhibitory cortical cells [Hz]	1.5		$w^o_{th\to rtn}$	Synaptic connection strength	12
α_{th}	mean rate constant – thalamic neurons [Hz]	0.2		$w^o_{rtn\to th}$	Synaptic connection strength	12
α_{rtn}	mean rate constant – reticular cells [Hz]	0.2		$\sigma^2_{e\to e}$	Synaptic connection range [mm]	0.1
a	Neural adaptation rate constant [Hz]	0.005		$\sigma^2_{e\to i}$	Synaptic connection range [mm]	0.1
b	Neural adaptation gain [1/s]	0.1		$\sigma^2_{i\to e}$	Synaptic connection range [mm]	2.5
I_e	Constant current bias [mV/s]	0		$\sigma^2_{i\to i}$	Synaptic connection range [mm]	2.5
I_i	Constant current bias [mV/s]	0		$\sigma^2_{e\to th}$	Synaptic connection range [mm]	0.1
I_{th}	Constant current bias [mV/s]	0.1		$\sigma^2_{e\to rtn}$	Synaptic connection range [mm]	0.1
I_{rtn}	Constant current bias [mV/s]	-0.5		$\sigma^2_{th\to e}$	Synaptic connection range [mm]	2.5
τ_{th}	Thalamo-cortical delay [ms]	2		$\sigma^2_{th\to i}$	Synaptic connection range [mm]	2.5
τ_{rtn}	Reticular-thalamic delay [ms]	2		$\sigma^2_{th\to rtn}$	Synaptic connection range [mm]	2.5
c	Conduction velocity [m/s]	0.35		$\sigma^2_{rtn\to th}$	Synaptic connection range [mm]	2.5
				dt	Integration time step [ms]	1

304

305 **Spiking occipital model**

306 The network topology of the occipital model is identical to that of the frontal model. However, by
307 virtue of the differences in intra-area neural structures and their different functional role in the
308 brain, some parameters are different. The time scale of the intra-cortical excitatory and inhibitory
309 adaption currents are chosen differently to

310 $$a_e^{-1}\frac{dv_e^j(t)}{dt} = -v_e^j(t) + u_e^j(t) \;;\; a_i^{-1}\frac{dv_i^j(t)}{dt} = -v_i^j(t) + u_i^j(t)$$

311 with $a_e = 1.0, a_i = 0.1$. This specific parameter choice in the full parameter set fixes the oscillation
312 frequency at large fluctuation variance to about 10Hz.

Effective mean-field model

To understand the macroscopic dynamics of the spiking neural network, it is insightful to consider its spatially averaged dynamics. Statistical features and average population dynamics of the cortical populations were exposed by investigating the mean-field formulation of the more fined grained spiking model above, leaving aside the LGN and reticular neurons. Using a mean-field approximation (26,27), the mean dynamics of the excitatory and inhibitory cortical potentials U_e and U_i can be shown to obey

$$\alpha_e{}^{-1}\frac{dU_e}{dt} = -U_e + bV_e + \bar{W}_{e\to e}F_e[U_e(t-\tau)] + \bar{W}_{i\to e}F_i[U_i(t-\tau)] + I_e \tag{4a}$$

$$\alpha_i{}^{-1}\frac{dU_i}{dt} = -U_i + bV_i + \bar{W}_{e\to i}F_e[U_e(t-\tau)] + \bar{W}_{i\to i}F_i[U_i(t-\tau)] + I_i \tag{4b}$$

$$a_e{}^{-1}\frac{dV_e}{dt} = -V_e + U_e \tag{4c}$$

$$a_i{}^{-1}\frac{dV_i}{dt} = -V_i + U_i\,, \tag{4d}$$

where the fluctuation-corrected neural response function reads

$$F_k[U] = \frac{1}{2}\left[1 + \mathrm{erf}\left(\frac{U-h}{\sigma_k\sqrt{2}}\right)\right] \quad ,$$

$$\sigma_k = -\sqrt{2}D\left(\frac{A^2}{2\lambda_+} + \frac{2AB}{\lambda_+ + \lambda_-} + \frac{B}{2\lambda_-}\right)$$

$$\lambda_\pm = (-a_k - \alpha_k \pm \sqrt{(a_k-\alpha_k)^2 + 4ba_k\alpha_k})/2\,,\ A = \sqrt{2\pi}\frac{a+\lambda_+}{\lambda_+-\lambda_-}\,,\ B = -\sqrt{2\pi}\frac{a+\lambda_-}{\lambda_+-\lambda_-} \quad .$$

Here, σ_k is the standard deviation of colored random fluctuations about the mean-field neural activity and each neuron behaves like a McCullogh-Pitts neuron with $\beta \to \infty$. Since $\sigma_k \sim D$, decreasing the fluctuation variance renders the response function F_k steeper. Previous studies

have shown that this may diminish the frequency of synchronous oscillation (26). The coefficients $\overline{W}_{n\to m}$ stand for the mean synaptic connectivity weights, computed by averaging all entries within the associated random matrices.

To understand the solution dynamics of the mean-field model, we have calculated numerically the stationary state of the mean-field model $(\overline{U}_e, \overline{U}_i, \overline{V}_e, \overline{V}_i)$ and studied numerically the temporal dynamics of deviations $(u_e = U_e - \overline{U}_e, u_i = U_i - \overline{U}_i, v_e = V_e - \overline{V}_e, v_i = V_i - \overline{V}_i)$ from these states. Parameters used are $\overline{W}_{e\to e} = 2.21, \overline{W}_{e\to i} = 4.58, \overline{W}_{i\to e}$=-3.46, $\overline{W}_{i\to i} = -1.69, b = 0.1\ ,\ a_e = a_i = 5.0$, $\alpha_e = 50.0\ , \alpha_i = 100.0\ , I_e = 0.1, I_i = 0,\ h = 0.1\ .$

Spectral Analysis

In the neural model, neuro-electric activity corresponds to a spatial summation of localized electric potentials emanating from superficial cortical neurons. We modeled the electroencephalographic $EEG(t)$ signal as the weighted spatial average

$$EEG(t) = N_e^{-1} \sum_{k=1}^{N_e} \phi_e^k u_e^k(t) + N_i^{-1} \sum_{k=1}^{N_i} \phi_i^k u_i^k(t) \quad , \quad (5)$$

$\phi_{e,i}^k = [0,1]$ denote random, positive coefficients accounting for dispersion effects and other source of observational noise. Spectral analysis in the time-frequency domain was performed applying Morlet wavelet analysis with equidistant frequencies.

Spike rate and spike coherence calculation

The instantaneous firing rate is the estimated number of spikes of each neuron occurring in a time window of *5ms* . In our evaluation the spike rate depends on the linearly decreasing fluctuation

353 variance and we applied a sliding window of width $\Delta D = 0.01$. To evaluate statistically the change
354 of spike rate, we applied a non-parametric Kruskal-Wallis test with respect to the firing rate at
355 maximum fluctuation variance.

356 Mean spike coherence in the cortex was computed based on standard calculations (28), consisting
357 of two randomly selected neurons i, j within the cortical population, and binning their respective
358 responses over a given time window ΔT. Thus, for neuron j, $X_j^{bin}(k\Delta T) = 1$ if a spike occurred
359 during the interval $[k\Delta T, (k+1)\Delta T]$, and zero otherwise, where $k = T/\Delta\mathrm{T}$. Intra-area coherence
360 $\theta(\Delta T)$ was then computed using

$$\theta(\Delta T) = \frac{\sum_T X_i^{bin} Y_j^{bin}}{\sum_T X_i^{bin\,2} \sum_T Y_j^{bin\,2}}$$

361 for two spike trains X, Y in the same area. The spike activity under study is assumed to evolve on a
362 large time scale compared to the rapid spike dynamics. Consequently it is reasonable to average
363 θ over a time window of duration T . In order to evaluate the evolution of the spike coherence with
364 changing fluctuation variance relative to the maximum fluctuation variance, we consider the
365 relative spike coherence θ/θ_0 where θ_0 is the spike coherence with maximum variance D. In the
366 simulations, we choose 100 randomly chosen pairs of neurons in the cortical E-population with a
367 small time window $\Delta T = 5\mathrm{ms}$ and $T = 1\mathrm{s}$ ($\Delta D = 0{,}00005$ and a range of fluctuation variances of
368 $D = 0.01$ in Figs. S3 and S4). Smaller time intervals ΔT retain the given results qualitatively. The
369 significance test is non-parametric of Kruskal-Wallis type and verifies the significance of the spike
370 coherence at various fluctuation variances compared to the maximum fluctuation variance.

371 In addition to the intra-area spike coherence, we compute the cross spike coherence between two
372 different areas where X, Y are spike trains from the areas. The corresponding parameters are
373 identical to the case of intra-area spike coherence, but for 300 randomly chosen pairs of neurons
374 from the different populations. All given spike coherence estimates are ratios to the spike

coherence at the largest fluctuation variance. The Kruskal-Wallis test verifies the significance of cross coherences compared to cross coherences at the maximum fluctuation variance.

Spike Field Coherence

Spike Field Coherence (SFC) reflects the synchronization between spikes and corresponding electric potentials (29). To estimate the SFC in the cortex at large and small fluctuations, we compute it in both cases in a time window of 5s in the $\delta -$(0.5Hz-4Hz), $\theta -$(4Hz-8Hz), $\alpha -$(8Hz-12Hz) and $\beta -$(12Hz-20Hz) frequency band. This standard measure estimates the coherence between spikes and their corresponding electric potentials at the same cell averaged over all cells.

In addition, we estimate the spike-field coherence between cortical EEG and spiking activity in the LGN cells and the reticular cell. The corresponding cross-SFC represents the coherence between thalamic spikes and cortical EEG at the same time instant averaged over all cells.

Global phase synchronization

Phase synchronization (PS) is a measure of the phase consistency between two time series. In our case, the PS between two populations in the network model is obtained by comparing the phase between their respective mean potential activities. Typically PS is non-stationary and subject to random fluctuations. The instantaneous phase-locking value (PLV) represents a statistical estimate of the degree of constant phase relation between several time series in a certain time interval and a certain frequency band (30). In fact, the PLV is the instantaneous circular variance of the phase difference of two time series. We take up this definition and compute a global PS index (GPS) by (31)

$$GPS = \left| \frac{1}{N} \sum_{k=1}^{N} e^{-i\Delta\varphi_k} \right|^2 \quad ,$$

$\Delta\varphi_k$ is the phase difference in the time series pair k at a certain time instance and N is the number of phase pairs considered. In practice, typically one averages over a set of pairs and time instances in a certain time window. The Results section shows values of GPS gained by a Morlet wavelet transform in the frequency range [1Hz;20Hz] based on E-population Local Field Potentials down-sampled to a sampling frequency of 50 Hz. We have chosen randomly 20 pairs of neurons out of 100 fixed randomly chosen neurons and averaged over 10 independent trials.

Instantaneous phases are defined mathematically in the case of non-vanishing instantaneous amplitudes only and may be spurious for very low amplitudes. We define numerical phase values φ_l from single time series l in the E-population to be valid only if its amplitude exceeds a threshold. This threshold is set to be half of the amplitude of the space-averaged activity at the same time instance and frequency band. This conservative criterion reduces the number of spurious phase synchronization indices dramatically and hence ensures the validity of the GPS.

Results

Experimental Data

Figure 3A illustrates the characteristic temporal evolution of EEG obtained experimentally in two patients: (I) at the beginning of the surgery during light anaesthesia, (II) during deep anaesthesia and (III) during the awake phase after surgery. The spectral content of the EEG during the full course of surgery is shown in Fig. 3B. We note that before the start of anaesthetic administration, the EEG exhibits artefactual activity in the delta-frequency range, caused by movement and muscle activity. After the onset of propofol (cf. Fig.1C, red curve), oscillations in the β -band emerge and gradually slow down towards the alpha-band, cf. white dashed line in Fig. 1B. In both of these patients, the analgesic fentanyl was also given, and the subsequent maintenance of general

anaesthesia was achieved by the volatile agent sevoflurane. After several minutes of anaesthetic administration, the power peak frequency saturates in the α-frequency band while increasing its spectral power. Moreover, the initial high fentanyl concentration enhances activity in the δ-frequency band. At the end of surgery, the anaesthetic concentration decreases and the patient emerges back to full consciousness (outside the time interval shown in Fig. 1). This emergence phase is nicely reflected by an increase in the frequency of the peak power; from the α-range back to the β–frequency range, and then followed by a suppression of oscillatory power in that frequency band. There is also a decrease of power in the δ-frequency band. In these cases, the emergence phase qualitatively resembles a backward loss of consciousness phase transition. This oscillatory pattern is called the *smile* effect due to the spectrogram trajectory of the peak frequency. Notice that in both subjects, the oscillatory transition observed is similar despite the big differences in the anaesthetic concentrations.

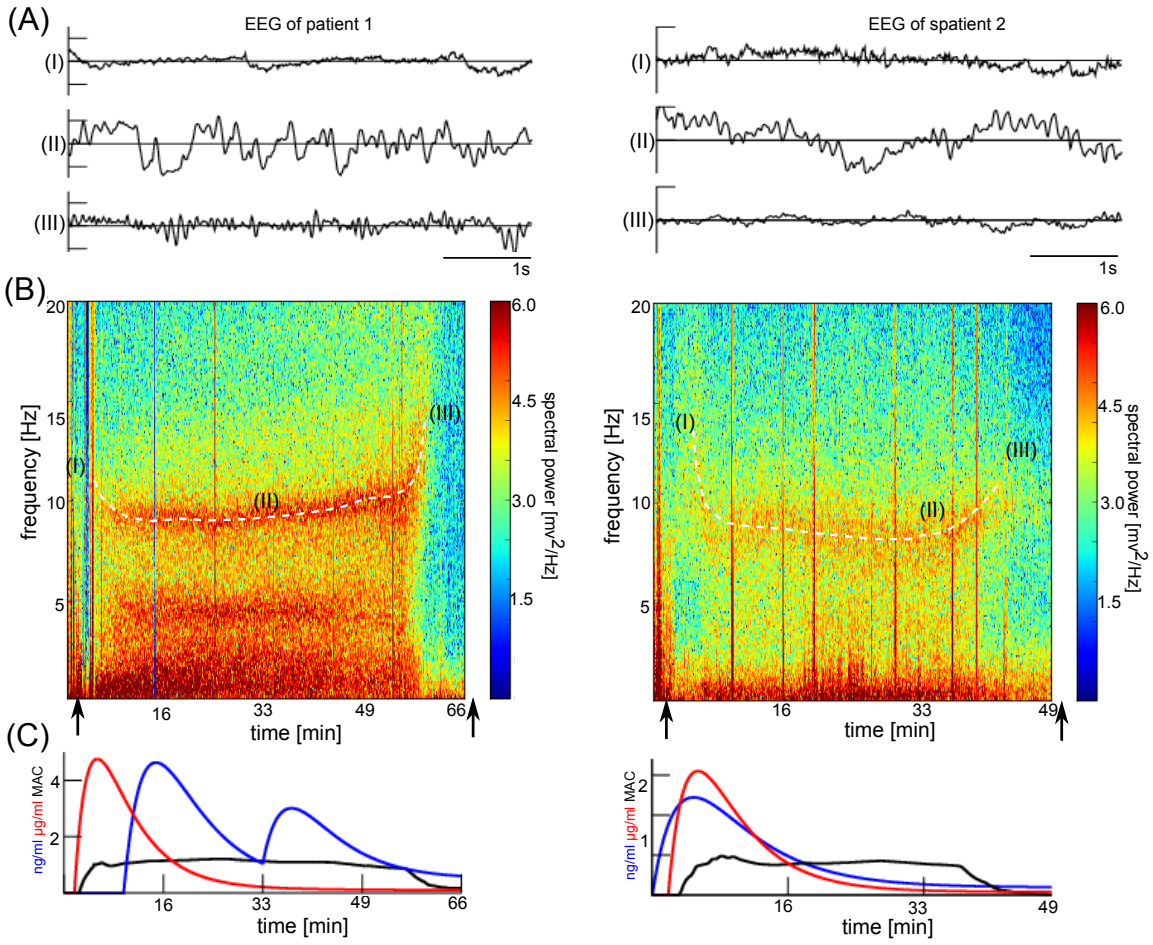

Figure 3: Characteristic *smile effect* observed in experimental frontal EEG spectral data. (A) Time series of experimental frontal EEG from two patients obtained at different moments in time during surgery, see (B) for encoded time points. (B) Spectral power distribution of experimental EEG data from two patients from the start to the end of surgery. The white dashed line denotes the frequency of maximum of α-activity illustrating the shape of a smile. (C) Estimated effect-site concentrations of the administered anaesthetic propofol (red), sevoflurane (black), and fentanyl (blue), over the time course of surgery. In each panel, the left and right arrows mark the point of loss of consciousness and emergence from unconsciousness in the subject, respectively. Unit of fentanyl concentration is ng/ml, unit of propofol concentration is μ g/ml and unit of sevoflurane is MAC (Minimum Alveolar Concentration).

Simulated EEG and neuronal spiking output from the frontal thalamo-cortical model

Broadband neural activity has been associated with large-scale connectivity motifs (32), whereas it has been suggested that increased neural fluctuation variance is the signature of a more segregated brain functional connectivity. Such segregated connectivity has been linked with increased correlated brain activity and spectral power (33). To represent the broadband activity in our model and in order to keep our results as generic as possible, we treated this exogenous broadband input in our model as random fluctuations; since the temporal and spatial correlation structure is not known.

In order to understand the role played by these broadband fluctuations on neural activity during anaesthesia, we analysed a thalamo-cortical neural model that exhibits the joint features of generic cortical and subcortical networks (Eqs. (4)). The action of anaesthetic drugs (e.g. propofol or sevoflurane) was modelled in two stages: fluctuation variance reduction, and synaptic inhibition. Firstly the fluctuation variance of exogenous inputs to the system ('neural noise') was decreased, cf. Fig. 4A (lower panel). The evolution and spectral properties of synchronous patterns were recorded for each epoch. This showed an induction of β-band activity followed by a generic deceleration of oscillatory activity, transitioning from the β band to the α band (Fig. 4A). An increase of the fluctuation level – as would occur when the concentration of anaesthetic drugs decrease – inverts the characteristic spectral features; giving rise to a spectrogram pattern like the characteristic anaesthetic "smile" in Fig. 2. The second modelled effect of anaesthetic drugs was to follow much previous literature and cause an increase in inhibitory synaptic gain. Figure 2B reveals that additional synaptic anaesthetic action does not qualitatively change the simulated EEG.

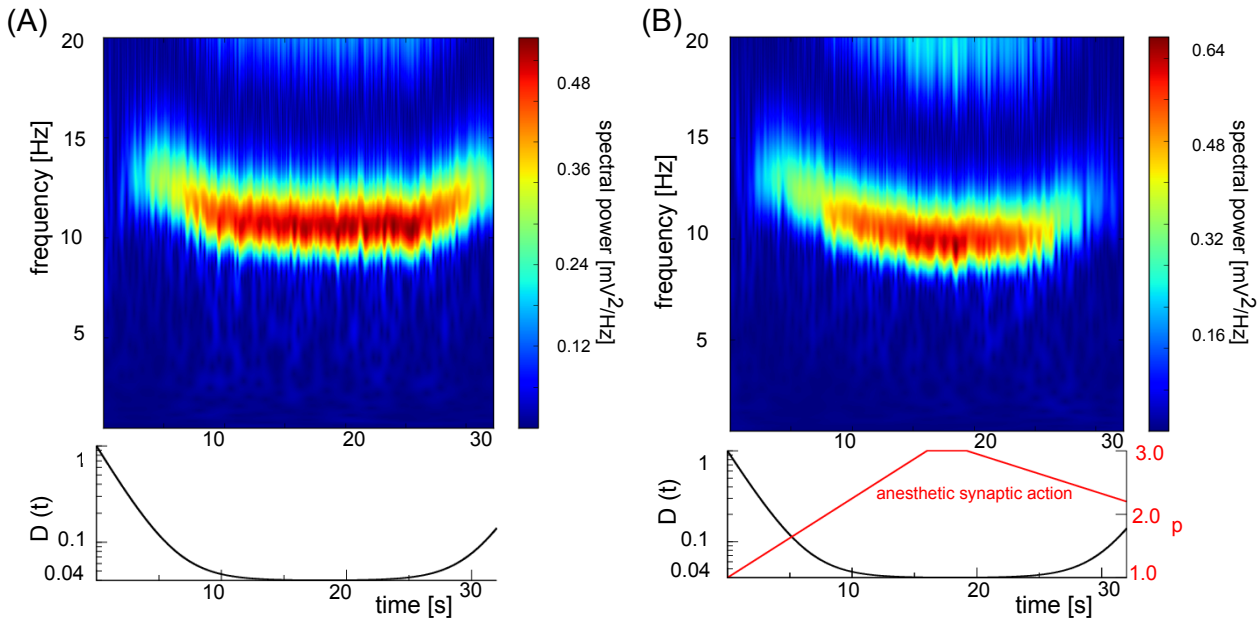

Figure 4: Numerical simulation of frontal EEG based on the frontal spiking neuron network model. (A) global drive by random fluctuations (B) global drive by random fluctuations with additional anaesthetic synaptic action. Spectral power of EEG (top panel) is given together with time-dependent fluctuation variance (bottom panel) .

The latter results show that weakening fluctuations induce oscillations in the cortical dendritic activity. In parallel spikes synchronize rhythmically both the cortex and thalamus. Figure 5 illustrates this finding in the spiking activity of a subset of neurons in the spiking network model in the absence of anaesthetic synaptic action (A). Initially, at high fluctuation variance (left panels), spiking is irregular and asynchronous but becomes more regular after some time when fluctuation variance decreases (right panels). At minimum fluctuation variance, the cortical E-cells burst with an inter-burst rhythm of 9Hz. The thalamic LGN cells burst at a rate of 4.5Hz, i.e. half of the burst firing rate of cortical neurons, and they synchronize with every second burst of cortical neurons. Simulated EEG weakly synchronizes with cortical E cell spiking at large fluctuation variance, whereas it strongly synchronizes with E cell spikes at low fluctuation variance. Adding anaesthetic

synaptic action (B) aligns few cortical spike trains in the E-population at low fluctuation variance. The aligned spike trains exhibit sparse burst activity; much less synchronous than under absence of anaesthetic synaptic action. LGN cells cease to spike regularly and almost stop spiking due to the increased synaptic inhibition. Similar to (A), EEG still synchronizes well with E cell spiking activity.

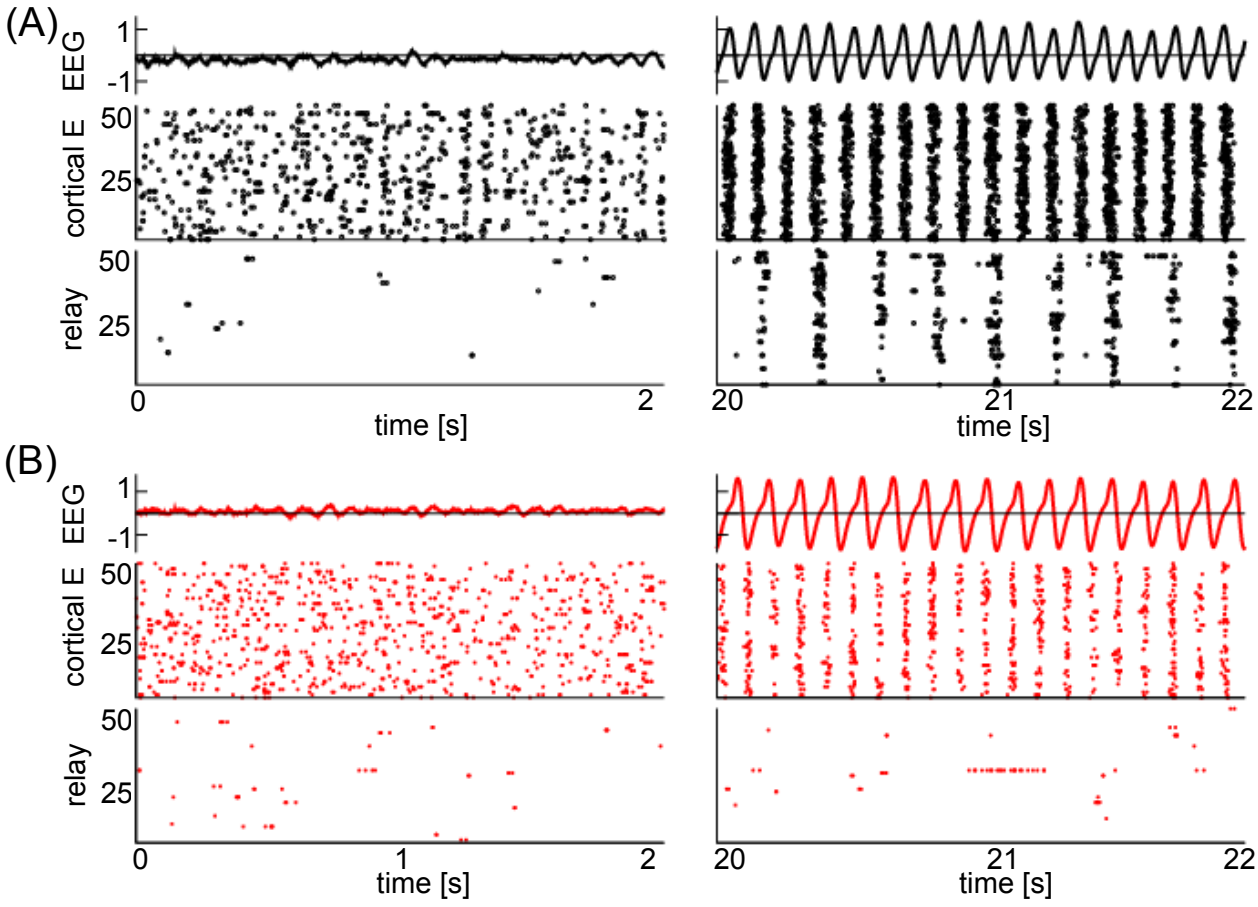

Figure 5: Increasing regularity of frontal EEG and spiking activity in frontal cortex and thalamus with increasing time and decreasing amplitude of random fluctuations. (A) global drive by random fluctuations (B) global drive by random fluctuations with additional anaesthetic synaptic action. The fluctuation level decreases according to Fig. 2, bottom panel. For better visualization, panels show spike events of 50 neurons only arbitrarily chosen in each neural structure. 'E' = excitatory neurons. 'relay' = thalamo-cortical relay neurons in the LGN.

493 *Mean-field spectra and connectivity in the frontal model*

494 Encephalographic activity represents the collective activity of neurons populating superficial
495 cortical networks. To understand better the fluctuation-induced spectral change observed in Figs. 3
496 and 4, we performed a mean-field analysis of a reduced cortical spiking network subjected to
497 additive noise.

498

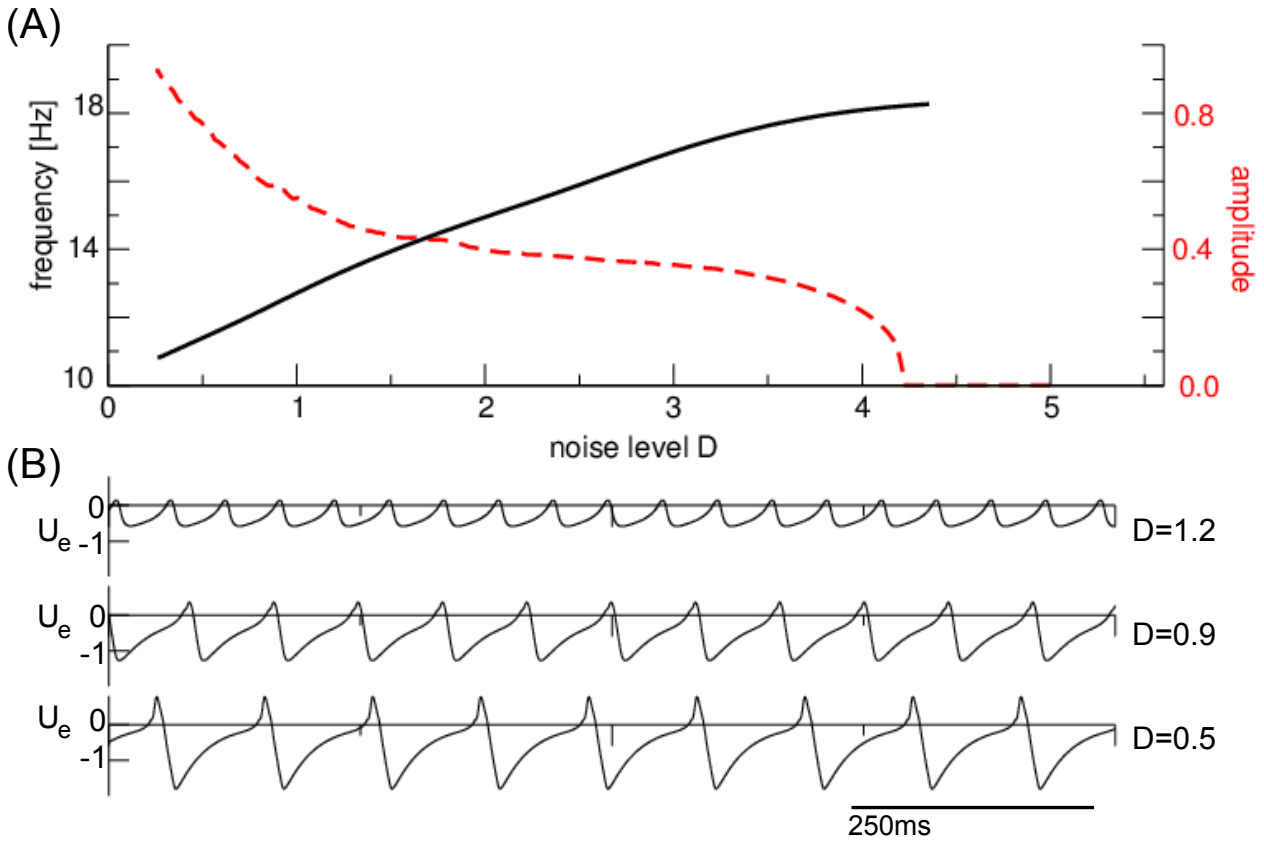

499
500 Figure 6: Random fluctuation-induced smile effect originates from an underlying oscillatory
501 instability (Hopf bifurcation). (A) The amplitude (red) and frequency (black) of deviations $U_e(t)$
502 from the systems stationary state are computed numerically based on the mean-field model, see
503 Eqs. (5). The large value of D compared to Fig. 4 and 5 compensates for the missing fluctuations
504 input from the thalamus – which is included in the full spiking model. (B) Simulated mean-field EEG
505 subjected to different noise levels.

We find that, at high fluctuation levels (D>4.2), the system does not oscillate and deviations from the stationary state have zero amplitude, cf. Fig. 6. Decreasing the fluctuation level induces loss of stability (Hopf bifurcation) resulting in increasing amplitude, initially in the β-band, but then slowing to the α-band. A noise-induced instability has been found recently in more simple neural models (39). Hence additive fluctuations alone are able a produce a shift in the network stability which is reflected by the observed changes in the system frequency and oscillation amplitude. This explains the frequency and magnitude tuning by modified fluctuation variance in the full model observed in Figs. 3-5.

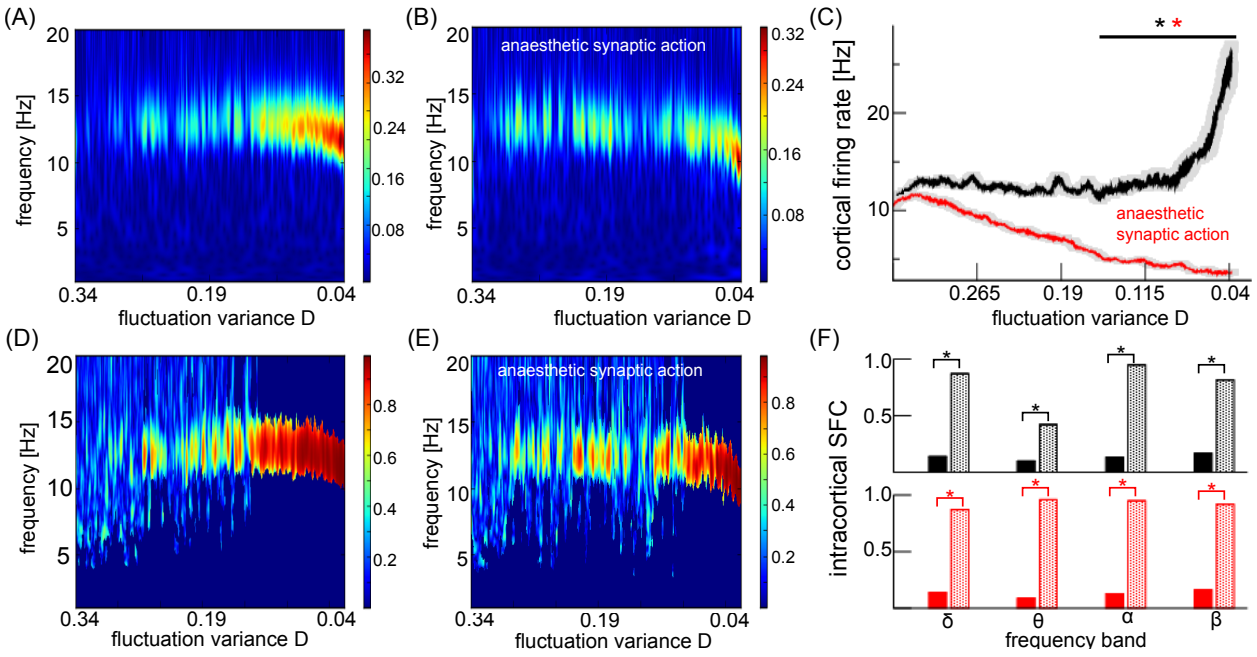

Figure 7: Spectral power, firing rate and synchronization in the frontal cortex with decreased fluctuation variance. (A) Power spectrum without anaesthetic synaptic action. (B) Power spectrum with anaesthetic synaptic action. (C) Mean population firing rate of E-cells. Error bars (grey) denote standard errors, firing rates below the horizontal bar are significantly different to firing rates at largest fluctuation variance ($p<0.001$, Kruskal-Wallis test) (D) Global phase synchrony of simulated LFPs without anaesthetic synaptic action. (E) Global phase synchrony of simulated LFPs with

anaesthetic synaptic action. (F) Intra-area spike-field coherence between E-cells, error bars denote standard errors. For all panels, the fluctuation variance D varies according to Fig.4, bottom panel.

Connectivity in the frontal network model

To better illustrate intra-cortical dynamics, Fig. 7 shows the spectral power (A) and the population firing rate (C, black) of dendritic activity in the modelled cortical excitatory neuronal population without synaptic anaesthetic action. The power and the firing rate ($p<0.001$) increases as the fluctuation variance decreases. The corresponding intra-area phase locking index of dendritic activity (D) between excitatory cells in the cortical area reveals a monotonic phase synchronization enhancement as fluctuation variance decreases. Similarly, weakening fluctuations enhances the intra-area SFC (F, black) in all frequency bands dramatically. This increase of intra-area SFC coincides with increasing phase synchrony (see panel D) when the peak of maximum spectral EEG power (panel a) shifts from the β-band to the α-band.

Considering anaesthetic action on the inhibitory synaptic gain in addition, the power surge (B), phase synchrony (E) in the β-and α-band and SFC (F, red) are retained; but we now see a more realistic statistically significant ($p<0.001$) decrease in the population firing rate (C, red). This decrease of firing rate is in line with experimental findings in the cortex in the presence of various anaesthetic agents (21).

The cross-spike-field coherence (CSFC) *between* different populations behaves differently. Weakening fluctuations markedly *diminishes* the coherence between cortical excitatory cells and thalamic cells as seen in Fig. 8. In the absence of inhibitory synaptic anaesthetic action, low fluctuation variance makes the CSFC vanish in all frequency bands except for the α-band where it increases in the α-band. The addition of inhibitory synaptic anaesthetic action to the model

545 eliminates the spike-field coherence in all frequency bands. Hence cortex and thalamus functionally
546 decouple.

547

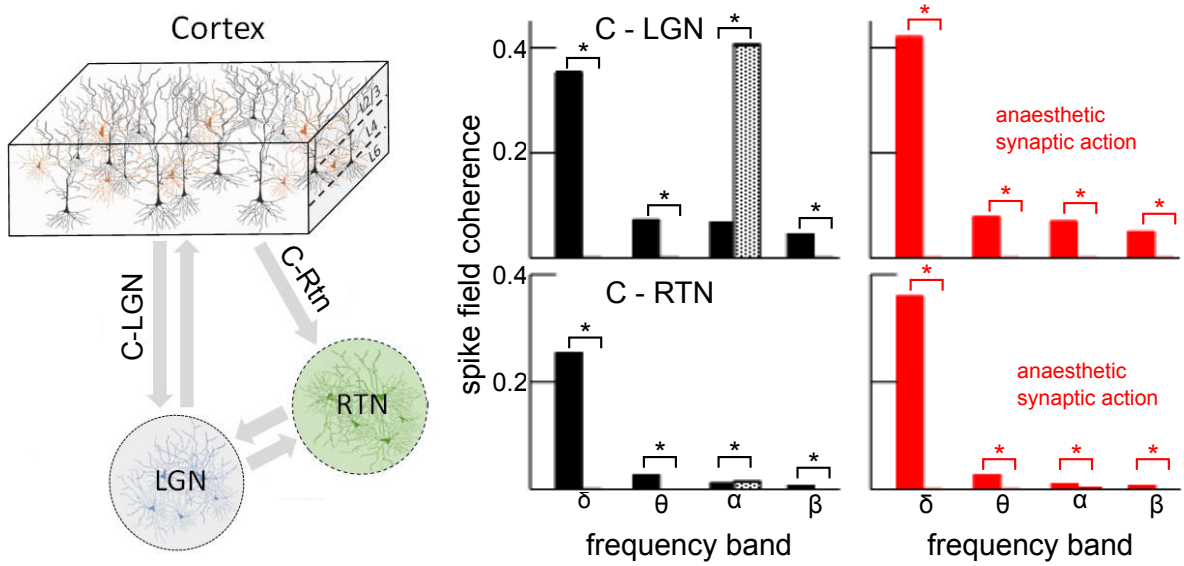

548

549 Figure 8: Frontal cortex and the thalamic structures decouple for weak random fluctuations. Panels
550 on right hand side show the cross spike-field coherence between cortex and LGN (C-LGN) and
551 between the cortex and the thalamic reticular area (C-RTN) subject to the fluctuation intensity in
552 the absence (black) and presence (red) of anaesthetic synaptic action. Error bars denote standard
553 errors, $p<0.0001$ (Kruskal-Wallis test)

554

555 *Anteriorisation : EEG and intra-area connectivity in the occipital thalamo-cortical model*

556 Anaesthetics are known to not only modify frontal EEG but synchronously occipital EEG (16,35,50).
557 Figure 9(A) shows strong activity in the α-band in the beginning (large fluctuation variance) that
558 drops rapidly after some time (small fluctuation variance). This transition is in good accordance to
559 experimental data (16,35). Since this posterior α-activity drops while the anterior α-activity

emerges (see previous sections), this effect is called anteriorization (50). The occipital α -rhythm emerges from a highly synchronous E-population (Fig.9(B)) that retains its phase synchrony over time, i.e. for all fluctuation variances. The high initial α -power is accompanied by synchronous spiking in the E-population (at large fluctuation variance), whereas spiking stops at large times (low fluctuation), cf. Fig. 9(C). At a first glance, this seems to contradict the persistent strong phase synchrony between the cells. However, thalamic LGN cells spike highly synchronous persistently over time at a frequency of ~10Hz driving the E population. This thalamo-cortical drive ensures the strong E-cell phase synchrony.

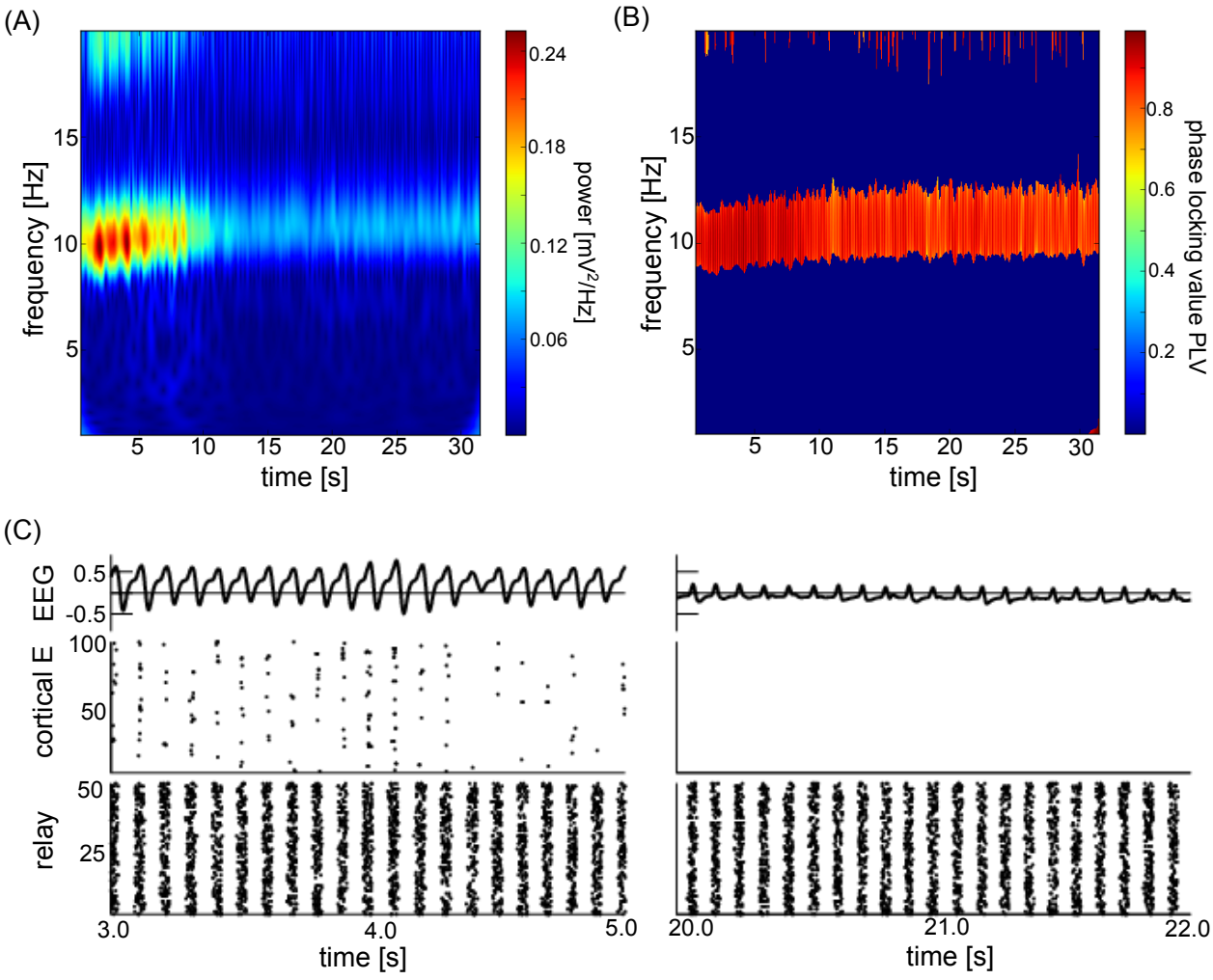

Figure 9: Occipital α -activity drops with increasing fluctuation variance while LGN activity is retained. (A) Time-frequency distribution of numerically simulated EEG. (B) Global phase synchrony in the E population. (C) EEG time series (top panel), spiking activity in a subset of 100 cortical E cells (centre panel) and in a subset of 50 LGN cells (bottom panel).

To understand better network interactions under anaesthesia, it is insightful to take a closer look at inter-area connectivity. Figure 10 reveals the fragmentation of occipital cortex and the thalamic areas PGN and RTN.

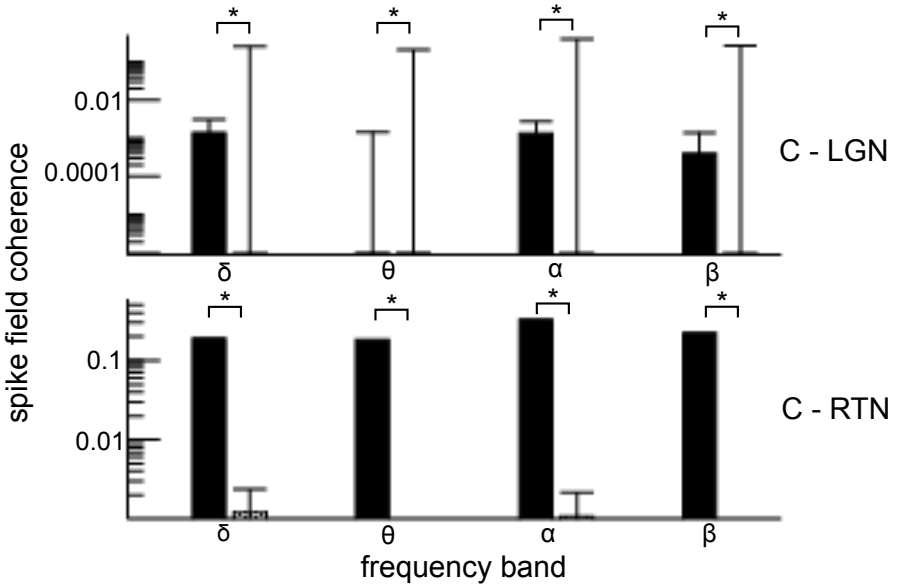

Figure 10: Inter-area connectivity between occipital cortex and the thalamic areas in different frequency bands. The solid and dotted bars denote the median spike field coherence (SFC) at high (D=1.0) and low (D=0.01) fluctuation variance, vertical bars denote the standard error. All SFC distributions in all frequency bands at high and low fluctuation variances are significantly different ($p<0.00001$).

.....

Discussion

584 **Model description of experimental EEG data**

585 The model we propose here is able to reproduce a number of observed characteristics of
586 propofol/sevoflurane anaesthesia. It describes the characteristic changes in EEG power and
587 frequency in the β- and α- frequency range, the increase in local neuronal intra-population
588 synchrony combined with loss of distant neuronal inter-population synchrony, and the decrease in
589 neuronal firing rate.

590

591 Previous experimental studies on the effect of general anaesthetics have shown an initial induction
592 of enhanced neural activity in the β frequency range with a subsequent peak frequency decrease to
593 the α-frequency band – the so-called smile effect or travelling peak mechanism (34) – with
594 changing anaesthetic concentrations (13, 16, 17, 35). Examples of this phenomenon are shown in
595 Figure 3. During this transition subjects typically lose consciousness. In recent years, many studies
596 have focussed on the reverse transition from unconsciousness back to consciousness and usually
597 revealed a reversal of these spectral characteristics (15, 35).

598

599 Our results show that time-frequency characteristics in the β and α frequency range can be
600 explained by a state-dependent change in broadband neural activity. The onset of β-activity and the
601 subsequent frequency decrease into the α-range can be explained by a transition from a stable to an
602 unstable oscillatory neural state, cf. Fig. 6.

603 The intra-population phase synchrony of the model EEG increases with decreasing fluctuation
604 intensity (Fig. 6) both in the absence and presence of anaesthetic inhibitory synaptic effects. This is
605 in line with experimental findings of enhanced EEG-coherence in the α band at large dose of
606 propofol (16).

607

608 Unlike the EEG patterns – which seem to be largely driven by levels of neural fluctuations –

609 neuronal ensemble spiking activity is more sensitive to the anaesthetic enhancement of inhibitory
610 synaptic effects. When the input fluctuations weaken cortical neurons start bursting synchronously,
611 but their synchrony weakens with increased anaesthetic inhibitory synaptic action (Figs. 5 and 7).
612 This is also reflected in their population firing rate which first decreases, but subsequently
613 increases as fluctuation variance is further decreased (if no anaesthetic synaptic action is included
614 in the model). Conversely the population firing rate decreases monotonically if increasing
615 anaesthetic synaptic inhibition is added to the model. These different effects indicate that it is the
616 relative level of fluctuation variance and anaesthetic inhibitory synaptic action that determines the
617 population firing rate. This finding corroborates the results of a previous experimental study (17)
618 which showed a wide range of firing rates in the prefrontal cortex after LOC in different patients –
619 both below and beyond the firing rate measured before LOC.
620
621 Relay cells in the LGN exhibit synchronous bursts in the absence of anaesthetic synaptic action. This
622 is in line with the burst activity observed experimentally in thalamic LGN neurons of un-
623 anaesthetized animals (36) and in non-REM sleep stages (37). Such burst-like activity in the LGN
624 has been postulated to block meaningful information transfer to the cortex (38). However under
625 anaesthetic synaptic action, LGN cells reduce their firing activity dramatically (Figs. 5 and 7).
626
627 One of the strengths of our approach is that the phenomenon we describe is fundamentally driven
628 by changes in pre-synaptic firing rates while assuming a generic neuron model. Hence the results
629 are robust to variations in neuron model parameters and does not require fine tuning. The
630 population dynamics predicted by our model are diverse and comprise both irregular firing and
631 bursting, originating from circuit interaction. This can be generated and altered in many ways, and
632 thus does not depend specifically on the neuron model we have chosen; or indeed the specific
633 neuronal effects of each different anaesthetic drug.

634

635 **Link between anaesthetic action and intrinsic fluctuation variance**

636

637 Using human data, and building on the well-known experimental finding that most anaesthetics
638 affect single neurons and populations by specific receptor and ion channel action (21), our work
639 departs from previous modelling studies by introducing the notion that a *generic decrease in neural*
640 *fluctuations* in the global brain network originating in the ascending arousal system may tune the
641 transitions observed under anaesthesia. A converging line of evidence indicates that anaesthesia
642 enhances the overall inhibition in the brain stem, which triggers a reduction in random input to the
643 cortex and the thalamus (39). In the current debate on the question of whether general anaesthetics
644 act primarily at cortical or subcortical levels, our model would lend support to the importance of
645 subcortical actions. It would also suggest that a progressive frontal increase in α-frequency as
646 anaesthesia concentration decreases at the end of surgery, could be a biomarker of gradual increase
647 in AAS activity, that is associated with a good post-operative recovery (40). This is also supported
648 by our finding that decreasing AAS induces a drop of α-power in occipital areas in very good
649 accordance to experimental data (16,35). Conversely, failure to show an increase in peak frequency
650 before waking might be an indication that the subcortical structures have not activated in the
651 correct order and are unprepared for the arousal – and hence is associated with more
652 postoperative delirium.

653

654 **Intra- and inter-area functional connectivity**

655

656 Large random fluctuations in a system result in broadband neural activity, which is associated with
657 large-scale connectivity motifs involving a plurality of time scales (32). This allows brain circuits to
658 explore their dynamic repertoire (41). Figure 7 reveals strong increases in phase synchrony of

electric potentials in the α-band *within* the cortical population at low fluctuation variance (i.e. during anaesthesia); which agrees with experimental studies demonstrating strong synchronized frontal α-activity close to the point of loss of consciousness (16, 35) and increased regional synchrony under sedation (52,53). The intra-area neuronal spike-field coherence quantifies functional connectivity based on the synchrony between spikes and co-localized electric potentials. Weak input fluctuations yield high coherence between cortical cells both with and without the inclusion of anaesthetic synaptic action in the model.

Considering inter-area connectivity, the cross-spike-field coherence between cortical and thalamic areas vanishes at low fluctuation variances with anaesthetic synaptic action, cf. Fig. 8, indicating a functional isolation of cortex from thalamus during anaesthesia. Such a decoupling between cortical and subcortical populations has been hypothesized theoretically (42) and adds to a growing body of evidence in sleep (42) and in anaesthesia (17, 43). Our results thus supports that de-noising the brain functionally decouples it and hence renders it more regular. This aligns with recent experimental results (44): studying local field potentials in ferrets under anaesthesia, the authors found reduced information transfer between prefrontal cortex and visual cortex with increased anaesthetic concentration. This decrease was associated with augmented active information storage (AIS) and reduced differential entropy (DE) in each area. Large AIS represents much stored information while low DE reflects less available information to be transferred. In this information theoretic framework, the enhanced intra-area functional connectivity observed experimentally in EEG and found in our model as augmented phase synchrony represents increased AIS and hence reduces the information that can be transferred. Moreover, a previous functional magnetic resonance imaging study (45) found a reduced repertoire of internal brain states under propofol anaesthesia. This is in line with the increased AIS and with suggested role of broadband neural activity in exploring the dynamical repertoire of neural networks (41). In addition, these results are

in agreement with the reported fact that random fluctuations - or neural variability - is beneficial to information processing and, consequently, less variability reduces the information flow between neural structures (46). Taken together, our work complements these studies by showing that weakening fluctuations not only hampers information flow between neural populations but consequently splits up interconnected networks.

In sum, our results show that weak fluctuations in the brain circuit cause a nonlinear oscillatory instability, yielding a local intra-area synchrony in the α frequency band. This intra-area synchrony disrupts synchrony between cortex and thalamus and hence fragments the various populations involved. Since the LGN is the relay structure of information flow, we conclude that its synchrony loss to the cortex contributes primarily to the loss of consciousness.

Perspectives of the model

Other studies on the origin of sleep-wake transitions have highlighted the importance of the AAS (47) controlling the brain excitation level. Various specific aminergic and cholinergic nuclei of the AAS originate in the brainstem and innervate both the cortex and the thalamus, activating LGN neurons as well as the reticular nuclei. Our proposed model takes into account noisy thalamic and cortical input assuming that broadband neural activity in the thalamo-cortical system is controlled by the brainstem; but it could equivalently be considered as coming from other uncorrelated distant cortical sources. This points to a synergistic interaction between the increased GABA effects of anaesthetic drugs and the decrease in neuronal fluctuations. The increased hyperpolarisation in distant brain structures, caused by the GABAergic actions, *will themselves* cause decreased fluctuations in the input to the region of brain under consideration. Thus the observed changes in EEG pattern might be secondary to GABAergic actions at a distant region. As an aside, the model proposed fits well with the known effects of ketamine on the EEG. This drug causes an increase in

alpha frequency and then loss of α-power, presumably the result of its known effect of increasing brain stem noise input to the thalamus and cerebral cortex. However the causes of ketamine-induced cortical segmentation are not explained by our model, and remain an enigma.

The proposed spiking population model and the derived mean-field model consider homogeneous spatial neural populations. This homogeneity approximation is valid for describing EEG spectra (33). More detailed experimental studies focussing on the spatio-temporal evolution of Local Field Potentials in rats under isoflurane anaesthesia have discovered a sequence of meta-stable neural states during the emergence phase (48). These meta-stable states are spatial patterns that are activated in a specific temporal sequence. Since meta-stable states require specific non-homogeneous network interactions (49) while the present model network is homogeneous, such meta-stable states are not solutions of our model, but may be elements of future work.

Previous network studies of coupled individual neurons have also reproduced qualitatively frontal and EEG (8) and anteriorisation (50) by considering anaesthetic effects in individual neurons. Even neural mass network models have been shown to reproduce both frontal EEG spectral features and anteriorisation (51). To our best knowledge, the present study is one of the first to involve the AAS demonstrating its importance. We have considered both frontal and occipital cortical areas, but have neglected other brain areas that are known to exhibit diverse anaesthetic impact. Examples are the parietal cortex and the areas of the default mode network that respond differently at different anaesthetic depths (52,54). Moreover the work does not consider deep anaesthesia where other characteristic features emerge such as burst suppression, slow frequencies (<1Hz), an intra-area fragmentation (52) or isoelectric activity (55).

As a conclusion, the present work proposes that anaesthetic action modifies the global regularity of

734 intrinsic neural activity. Increasing anaesthetic concentration decreases broadband fluctuations,
735 enhances the coherence of intra-area neural activity, and induces a functional decoupling of the
736 thalamo-cortical circuit. The parallel increase in intra-area functional connectivity accompanied by
737 a reduction of functional connectivity between network areas is a direct consequence of amplified
738 correlations in neural activity.
739

740 Acknowledgements

741 This work has been supported by the Natural Sciences and Engineering Research Council of Canada
742 (JL).
743

744 Contributions

745 All authors designed the study, analysed the data, and wrote the paper.
746

747 Competing interests

748 We state that there are no competing interests.

749 Declaration of interests:

750 None.

751

752

753 References

754 1. Grasshoff C, Drexler B, Rudolph U and Antkowiak B (2006). Anaesthetic drugs: linking molecular
755 actions to clinical effects. *Curr. Pharm. Des.* 12(28) : 3665-3679

756 2. Alkire MT, Hudetz AG and Tononi G (2008). Consciousness and Anesthesia. *Science* 322 : 876 -
757 880. doi :10.1126/science.1149213

758 3. Sellers K, Bennett D, Hutt A, Williams J and Frohlich J (2015). Awake versus Anesthetized: Layer-
759 Specific Sensory Processing in Visual Cortex and Functional Connectivity between Cortical Areas, *J.*
760 *Neurophysiol.* 113(10): 3798-815.
761 4. Barttfeld P, Uhrig L, Sitt JD, Sigman M, Jarraya B and Dehaene S (2015) Signature of
762 consciousness in the dynamics of resting-state brain activity, *Proc. Natl. Aca. Sci. USA* 112(3) : 887-
763 889. Doi : 10.1073/pnas.1418031112

764 5. Schultz A, Siedenberg M, Grouven U, Kneif T and Schultz B (2008). Comparison of Narcotrend
765 Index, Bispectral Index, spectral and entropy parameters during induction of propofol–remifentanil
766 anaesthesia, *J. Clin. Monit. Comput.* 22 :103–111.

767 6. Hight D, Voss LJ, Garcia PS and Sleigh J (2017). Changes in Alpha Frequency and Power of the
768 Electroencephalogram during Volatile-Based General Anesthesia. *Front. Syst. Neurosci.* 11 :36. doi :
769 10.3389/fnsys.2017.00036

770 7. McCarthy MM, Brown EN and Kopell N (2008). Potential Network Mechanisms Mediating
771 Electroencephalographic Beta Rhythm Changes during Propofol-Induced Paradoxical Excitation. *J.*
772 *Neurosci.* 28(50) : 13488-13504.

773 8. Ching S, Cimenser A, Purdon PL, Brown EN and Kopell NJ (2010). Thalamocortical model for a
774 propofol-induced-rhythm associated with loss of consciousness. *Proc. Natl. Acad. Sci. USA* 107(52):
775 22665-22670.

9. Bojak I, Day HC and Liley DTJ (2013). Ketamine, propofol, and the EEG: a neural field analysis of HCN1-mediated interactions. *Front. Comput. Neurosci.* 7: 22

10. Hashemi M, Hutt A and Sleigh S (2014). Anesthetic action on extra-synaptic receptors: effects in neural population models of EEG activity. *Front. Syst. Neurosci.* 8, 232. doi: 10.3389/fnsys.2014.00232

11. Hendrickx JF, Eger EI, Sonner JM and Shafer SL (2008). Is synergy the rule? A review of anesthetic interactions producing hypnosis and immobility. *Anesth. Analg.* 107(2) :494-506 . doi: 10.1213/ane.0b013e31817b859e

12. Steriade M, Amzica F, Contreras D (1994). Cortical and thalamic cellular correlates of electroencephalographic burst-suppression. *Electroencephalogr. Clin. Neurophysiol.* 90:1-16.

13. Sellers KK, Bennett DV, Hutt A and Fröhlich F (2013). Anesthesia differentially modulates spontaneous network dynamics by cortical area and layer. *J. Neurophysiol* 110:2739-2751. doi:10.1152/jn.00404.2013

14. Hudetz AG, Liu X, Pillay S, Boly M, Tononi G (2016). Propofol anesthesia reduces Lempel-Ziv complexity of spontaneous brain activity in rats. *Neurosci Lett.* 628:132-5. doi: 10.1016/j.neulet.2016.06.017

15. Vizuete JA, Pillay S, Ropella KM and Hudetz AH (2014). Graded Defragmentation of cortical neuronal firing during recovery of consciousness in rats. *Neuroscience* 275 : 340-351. doi : 10.1016/j.neuroscience.2014.06.018

16. Cimenser A, Purdon PL, Pierce ET, Walsh JL, Salazar-Gomez AF, Harrell PG, Tavares-Stoeckel C, Habeeb K and Brown EM (2011) Tracking brain states under general anesthesia by using global coherence analysis , *Proc. Natl. Aca. Sci. USA* 108(21) : 8832–8837. doi: 10.1073/pnas.1017041108

17. Lewis LD, Weiner VS, Mukamel EA, Donoghue JA, Eskandar EN, Madsen JR, Anderson WS Hochberg LR, Cash SS, Brown EN and Purdon PL (2012) Rapid fragmentation of neuronal networks at the onset of propofol-induced unconsciousness. *Proc. Natl. Acad. Sci. USA*109(49):19891–19892. doi: 10.1073/pnas.1210907109

18. Alkire MT and Miller J (2005). General anesthesia and the neural correlates of consciousness. *Prog Brain Res.* 150:229-44.

19. Brown EN, Lydic R and Schiff ND (2010) General Anesthesia, Sleep and Coma. *N. Engl. J. Med.* 363: 2638-2650.

20. Saper CB, Scammell TE, Lu J. (2005) Hypo-thalamic regulation of sleep and circadian rhythms. *Nature* 437:1257-63

21. Franks NP (2008) General anaesthesia: from molecular targets to neuronal pathways of sleep and arousal. *Nat Rev Neurosci.* 9(5):370-86. doi: 10.1038/nrn2372.

22. Kopanitsa MV (1997). Extrasynaptic receptors of neurotransmitters: distribution, mechanisms of activation, and physiological role. *Neurophysiol.* 29 : 448–458.

23. Mitchell SJ and Silver RA (2003) Shunting inhibition modulates neuronal gain during synaptic excitation. *Neuron* 38 : 433-445.

24. Hutt A and Buhry L (2014) Study of GABAergic extra-synaptic tonic inhibition in single neurons and neural populations by traversing neural scales: application to propofol-induced anaesthesia. *J. Comput. Neurosci.* 37(3) : 417-437 .

25. Amari S (1977) Dynamics of Pattern Formation in Lateral-Inhibition Type Neural Fields. Biol. Cybern. 27 : 77-87

26. Lefebvre J, Hutt A, Knebel JF, Whittingstall K and Murray M (2015). Stimulus Statistics shape oscillations in nonlinear recurrent neural networks. *J. Neurosci.* 35(7): 2895-2903

27. Herrmann C, Murray MM, Ionta S, Hutt A and Lefebvre J (2016) Shaping neural oscillations with

periodic stimulation. *J. Neurosci.* 36(9): 5328-37

28. Wang XJ and Buzsaki G (1996). Gamma oscillation by synaptic inhibition in a hippocampal interneuronal network model. *J. Neurosci.* 16(20) : 6402–6413

29. Fries P, Reynolds JH, Rorie AE, Desimone R (2001). Modulation of oscillatory neuronal synchronization by selective visual attention. *Science* 291(5508):1560-3.

30. Lachaux JP, Rodriguez E, Martinerie J and Varela FJ (1999). Measuring phase synchrony in brain signals. *Human Brain Map.* 8: 194-208

31. Hutt A and Munk MHJ (2007). Mutual phase synchronization in single trial data. *Chaos and Complexity Letters* 2 (2/3): 225-246.

32. Voytek B, Kayser AS, Badre D, Fegen D, Chang EF, Crone NE, Parvizi J, Knight RT and D'Esposito M (2015). Oscillatory dynamics coordinating human frontal networks in support of goal maintenance. *Nature Neurosci.* 18:1318-1324. doi: 10.1038/nn.4071

33. Deco G, Jirsa VK, Robinson PA, Breakspear M and Friston K. (2008). The dynamic brain: from spiking neurons to neural masses and cortical fields. *PLoS Comput Biol.* 4(8):e1000092. doi: 10.1371/journal.pcbi.1000092

34. Scheib MC (2017) Brainstem influence on thalamocortical oscillations during anesthesia emergence. Front. Syst. Neurosci. 11 :66 .

35. Purdon PL, Pierce ET, Mukamel EA, Prerau MJ, Walsh JL, Wong KFK, Salazar-Gomez AF, Harrell PG, Sampson AL, Cimenser A, Ching S, Kopell NJ, Tavares-Stoeckel C, Habeeb K, Merhar R and Brown EN (2012). Electroencephalogram signatures of loss and recovery of consciousness from propofol. *Proc. Natl. Acad. Sci. USA* 110(12): E1142–E1151

36. Sherman SM (2001). Tonic and burst firing: dual modes of thalamocortical relay. *Trends*

Neurosci. 24:122–126.

37. McCormick DA and Bal T (1997). Sleep and arousal : thalamocortical mechanisms. *Annu. Rev. Neurosci.* 20: 185–215.

38. Livingstone MS and Hubel DH (1981). Effects of sleep and arousal on the processing of visual information in the cat. *Nature* 291:554–561.

39. Zecharia AY and Franks NP (2009). General anesthesia and ascending arousal pathways. *Anesthesiology* 111(4):695-6. doi: 10.1097/aln.0b013e3181b061bc.

40. Chander D, Garcia PS, MacColl JN, Illing S and Sleigh JW (2014). Electroencephalographic variation during end maintenance and emergence from surgical anesthesia. *PLoS One.* 9(9):e106291. doi: 10.1371/journal.pone.0106291.

41. Ghosh A, Rho Y, McIntosh AR, Kötter R and Jirsa VK (2008). Noise during Rest Enables the Exploration of the Brain Dynamic Repertoire. *PLoS Comput. Biol.* 4(10) : e1000196. Doi : 10.1371/journal.pcbi.1000196

42. Tononi G, Boly M, Massimini M and Koch C (2014) Integrated information theory : from consciousness to its physical substrate. *Nature Rev. Neurosci.* 17 (7): 450–461. doi:10.1038/nrn.2016.44

43. Massimini M, Ferrarelli F, Huber R, Esser SK, Singh H and Tononi G (2005) Breakdown of Cortical Effective Connectivity During Sleep. *Science* 309 :2228.

44. Wollstadt P, Sellers KK, Rudelt L, Priesemann V, Hutt A, Frohlich F and Wibral MI (2017). Breakdown of local information processing may underlie isoflurane anesthesia effects. *PLoS Comp. Biol.* 13(6): e1005511. doi :10.1371/journal.pcbi.1005511

45. Hudetz AG, Liu X, Pillay S (2015) Dynamic repertoire of intrinsic brain states is reduced in

propofol-induced unconsciousness**.** *Brain Connect.* 5(1):10-22. doi: 10.1089/brain.2014.0230

46. Stein RB, Gossen ER and Jones KE (2005). Neuronal variability : noise or part of the signal ? *Nature Rev. Neurosci.* 6 :389-397. doi : 10.1038/nrn1668

47. Fuller P, Sherman D, Pedersen NP, Saper CB and Lu J (2011) Reassessment of the structural basis of the ascending arousal system. *J. Comp. Neurol.* 519(5): 933-956

48. Hudson AE, Calderon DP, Pfaff DW and Proekt A (2014). Recovery of consciousness is mediated by a network of discrete metastable activity states. *Proc. Natl. Acad. Sci. USA* 111(25): 9283–9288. doi: 10.1073/pnas.1408296111

49. Schwappach C, Hutt A and beim Graben P (2015). Metastable dynamics in heterogeneous neural fields. *Front. Syst. Neurosci.* 9:97. doi: 10.3389/fnsys.2015.00097

50. Vijayan S, Ching S, Purdon PL, Brown EN and Kopell NJ (2013). Thalamocortical Mechanisms for the Anteriorization of Alpha Rhythms during Propofol-Induced Unconsciousness. *J. Neurosci*. 33(27):11070 –11075

51. Hashemi M, Hutt A and Sleigh J (2015). How the cortico-thalamic feedback affects the EEG power spectrum over frontal and occipital regions during propofol-induced anaesthetic sedation. *J. Comput. Neurosci.* 39(1): 155

52. Huang Z, Liu X, Mashour GA and Hudetz AG (2018) Timescales of Intrinsic BOLD Signal Dynamics and Functional Connectivity in Pharmacologic and Neuropathologic States of Unconsciousness. J. neurosci. 38(9) :2304-2317.

53. Li D, Voss LJ, Sleigh JW and Li X. (2013) Effects of volatile anesthetic agents on cerebral cortical synchronization in sheep. *Anesth.* 119(1):81-8.

54 . Liu X, Pillay S, Li R, Vizuete JA, Pechman KR, Schmainda KM and Hudetz AG (2013) Multiphasic modification of intrinsic functional connectivity of the rat brain during increasing levels of propofol.

889 *Neuroimage* 83 :581-92

890 55. Altweg-Boussac T, Schramm AE, Ballestero J, Grosselin F, Chavez M, Leca S, Baulac M, Naccache
891 N, Demeret S, Navarro V, Mahon S, Charpier S (2017). Cortical neurons and networks are dormant
892 but fully responsive during isoelectric brain state. *Brain* 140:2381-2398.

893 56. Fuller PM, Sherman D, Pedersen NP, Saper CB and Lu J (2011) Reassessment of the Structural
894 Basis of the Ascending Arousal System. *J. Comp. Neurol*. 519:933–956.

895